*Article*

# Exploring Deep Learning for Adaptive Energy Detection Threshold Determination: A Multistage Approach

Oguz Bedir [1,*], Ali Riza Ekti [2] and Mehmet Kemal Ozdemir [3]

1. Graduate School of Engineering and Natural Sciences, Istanbul Medipol University, 34810 Istanbul, Turkey
2. Department of Electrical-Electronics Engineering, Balikesir University, 10145 Balikesir, Turkey; alirizaekti@gmail.com
3. Department of Computer Engineering, Istanbul Medipol University, 34810 Istanbul, Turkey; mkozdemir@medipol.edu.tr
* Correspondence: oguz.bedir@std.medipol.edu.tr

**Abstract:** The concept of spectrum sensing has emerged as a fundamental solution to address the growing demand for accessing the limited resources of wireless communications networks. This paper introduces a straightforward yet efficient approach that incorporates multiple stages that are based on deep learning (DL) techniques to mitigate Radio Frequency (RF) impairments and estimate the transmitted signal using the time domain representation of received signal samples. The proposed method involves calculating the energies of the estimated transmitted signal samples and received signal samples and estimating the energy of the noise using these estimates. Subsequently, the received signal energy and the estimated noise energy, adjusted by a correction factor (k), are employed in binary hypothesis testing to determine the occupancy of the wireless channel under investigation. The proposed system demonstrates encouraging outcomes by effectively mitigating RF impairments, such as carrier frequency offset (CFO), phase offset, and additive white Gaussian noise (AWGN), to a considerable degree. As a result, it enables accurate estimation of the transmitted signal from the received signal, with 3.85% false alarm and 3.06% missed detection rates, underscoring the system's capability to adaptively determine a decision threshold for energy detection.

**Keywords:** spectrum sensing; energy detection; deep learning; adaptive threshold

## 1. Introduction

Multiple entities, be they humans or machines, that participate in wireless communication should utilize the same, limited electromagnetic (EM) frequency spectrum that is allocated by the regulatory bodies to be used for certain wireless communication standards. On the other hand, the wireless communications field has been expanding in terms of both the number of users and application areas, and this trend appears to continue into the future [1]. This growth has been creating more demand to access the limited EM frequency spectrum, making it a scarce resource that must be efficiently managed to meet the demand [2].

The field of wireless communications has witnessed extensive research and implementation efforts to address the increasing demand for efficient and reliable communication systems. Various strategies have been explored, including, but not limited to, the utilization of cellular systems, advancements in multiplexing and multiple access techniques, the integration of radar sensing and communication functionalities [3–5], beamforming for spatial user separation [6], and the adoption of massive multiple-input multiple-output (MIMO) technology [7], to name a few.

The concept of cognitive radio (CR) has emerged as a promising solution with the potential to achieve efficient utilization of the electromagnetic frequency spectrum and transform the wireless communications protocol stack into a more adaptable system. By understanding its radio environment and making intelligent decisions in real time, CR

aims to address various user needs in different application scenarios [2,8]. Even though there are multiple facets to consider, such as spectrum sharing and management, spectrum-aware networking, sensing scheduling, joint software, and hardware design [9,10], to equip the radio with cognitive abilities, it can be claimed that sensing the spectrum with the purpose of identifying the opportunities, e.g., available time-frequency slots, in the spectrum space [11] is the initiator of the CR's capabilities. Thus, being an essential component of CR, spectrum sensing has attracted the interest of the research community.

It appears that this interest will persist. Based on the findings of [12], it has been observed that while 5G networks generally outperform 4G networks in terms of service quality and speed, their performance has diminished over time due to the increased number of users accessing 5G networks without a corresponding increase in network capacity. The primary limiting factor in addressing this capacity constraint is the scarcity of available EM spectrum resources. Considering the envisioned goals of 6G [13,14], which strive to establish ubiquitous connectivity across diverse vertical application domains, it can be inferred that the ongoing significance of efficient EM spectrum utilization persists. Consequently, the research topic of spectrum sensing retains its importance, as it directly addresses the need to effectively detect and allocate available spectrum resources in support of 6G's objectives.

Spectrum sensing research is often classified into two primary categories: wideband sensing and narrowband sensing. Wideband sensing can be further characterized by two distinct methodologies: Nyquist-based and sub-Nyquist-based methods. Similarly, narrowband sensing is investigated under two discrete classifications: coherent methods and non-coherent methods [15,16].

Nyquist-based wideband sensing methods often suffer challenges due to their reliance on high sampling rates, necessitating specialized and expensive equipment. In contrast, sub-Nyquist wideband sensing methods alleviate the aforementioned requirements. However, a substantial portion of these methods rely on assumptions of sparsity and the estimation of sparsity levels, thereby introducing high computational complexity [17]. An increase in computational complexity is frequently associated with increased energy consumption, which is particularly undesirable for radios operating in resource-constrained environments, such as mobile phones or military radios that are deployed in field conditions.

While wideband sensing methods offer the potential to sense a significantly broader spectrum in comparison with narrowband sensing methods, the latter, characterized by their relatively lower sampling rates, prove more compatible with conventional, non-bulky, cost-effective equipment, including mobile phones, software-defined radios, and military radio devices. Despite the generally high performance exhibited by coherent narrowband sensing methods, such as matched filtering and waveform detection, their notable drawback lies in the necessity of possessing either partial or complete prior knowledge of the primary signal characteristics, which is frequently unavailable.

Alternative narrowband sensing techniques, such as cyclostationary feature detection, covariance-based detection, etc., exhibit commendable performance even in challenging channel conditions. Nonetheless, these methods are encumbered by the drawback of high computational complexity. Energy detection is a non-coherent and straightforward narrow-band sensing technique that is widely adopted in the literature. It involves subjecting a test statistic to binary hypothesis testing against a threshold value. Its popularity stems from its low computational complexity and the absence of the need for prior knowledge about primary user signals. However, it exhibits limitations in terms of reliability at low signal-to-noise ratio (SNR) values and susceptibility to noise uncertainty. Finally, it is worth mentioning that artificial intelligence (AI)-based approaches have been leveraged either as standalone methodologies or in combination with the aforementioned techniques to yield enhanced and more efficient approaches [18]. In [19], a system is introduced that incorporates convolutional neural network (CNN) and long short-term memory (LSTM) deep learning (DL) architectures. CNN extracts energy-correlation features from sensing data covariance matrices, while LSTM utilizes these features across multiple sensing pe-

riods to learn the primary user activity patterns and enhance the detection probability. Notably, this approach operates without making assumptions about signal-noise models. In [20], researchers utilize short-time Fourier transform to create time-frequency matrices from the received samples, which serve as inputs for the CNN model used in spectrum occupancy classification. Effectively, this approach transforms the problem into an image classification task. The proposed method places no constraints on primary user signals and remains robust in the presence of SNR variations. Ref. [21] presents a system using spectral correlation function outputs as the input for a CNN. This approach not only determines channel occupancy, but also identifies the types of signals occupying the channel, demonstrating robustness even in challenging channel conditions. In [22], the authors employ power spectrum as the CNN input, normalizing received signal power to mitigate noise power uncertainty. They use the Residual Neural Network model, training it with an extensive dataset of signal and noise data. Transfer learning is applied, where the network is initially trained with simulated data and then fine-tuned with real-world signals. This method performs well under colored noise and exhibits the ability to generalize when detecting unknown signals. In contrast, Ref. [23] directly employs complex-valued samples as CNN inputs, eliminating the need for feature extraction. Transfer learning techniques are integrated to address performance degradation in diverse scenarios beyond the training dataset. Likewise, in [24], raw signals act as inputs for a neural network model, which includes one-dimensional CNN, bidirectional LSTM (BiLSTM), and self-attention (SA) components. This fusion utilizes CNN for local pattern extraction, BiLSTM for capturing long- and short-term dependencies, and SA for highlighting specific features.

In the context of energy detection, establishing a threshold that ensures a consistent false alarm rate and missed detection rate requires either having explicit information about the noise variance and SNR, or estimating these parameters from the available data. Extensive research has focused on the development of adaptive threshold determination methods, driven by the recognition that the noise floor commonly exhibits non-stationary behavior. The objective of these studies is to devise techniques that can dynamically adjust the threshold to accommodate the temporal fluctuations in the noise floor, enabling more robust and accurate detection performance.

For example, Ref. [25] introduces an adaptive thresholding method by leveraging the binarization concept used in image processing. The proposed approach represents the threshold as a linear function of the mean and standard deviation of the received signal samples. Ref. [26] proposes a heuristic method modeled as a linear function of the signal-to-interference-plus-noise-ratio. They highlight the simplicity and practicality of this approach for engineering applications. The authors also highlight that although the proposed method necessitates complex offline optimization, it offers straightforward online threshold control. Ref. [27] addresses the problem of minimizing the error decision probability by formulating it as a function of the primary user's spectrum utilization ratio (ranging from 0 to 1) and the threshold. The authors demonstrate that when the spectrum utilization ratio is fixed, the error decision probability function exhibits convex behavior, allowing for the derivation of solutions. A novel three-event energy detection algorithm is presented in [28]. The authors employ Newton's method with forced convergence in a single iteration to accurately approximate the optimal decision threshold, effectively minimizing the error decision probability. In [29], the authors present a novel approach centered on deep reinforcement learning. They employ a custom-designed reward function within the deep Q-network algorithm to intelligently adjust the energy detection threshold. Furthermore, they seamlessly integrate this method with a clustered cooperative spectrum sensing architecture, harnessing the collective power of these advanced techniques for enhanced spectrum management. In [30], the authors present a method for adaptive threshold determination, employing noise power estimates obtained at each sensing interval. The noise power estimation relies on the spectral minima tracking (SMT) technique. Furthermore, the authors perform a correlation analysis to assess the relationship between the parameters of the SMT technique and the resulting noise power estimates. Leverag-

ing the insights from this analysis, they fine-tune the parameters of the SMT method to enhance the accuracy of their noise power estimations. In their study, Ref. [31] enhance the fixed double-threshold using a conventional mean energy detection algorithm with a novel approach by determining the intermediate threshold adaptively. They formulate the intermediate threshold as a weighted combination of high- and low-value thresholds and employ a decision error probability metric to optimize its value.

With the primary objective of enhancing the utilization of the limited electromagnetic spectrum in real-world applications, this study introduces a novel multi-stage DL approach to spectrum sensing. It employs energy detection with adaptive thresholding, utilizing multiple stages of DL techniques applied to the time domain representation of the narrowband channel readings to estimate the threshold. The key contributions of the proposed approach are:

- The introduction of a multi-stage DL approach that effectively mitigates channel impairments and jointly conducts spectrum sensing while maintaining superior performance, resulting in low false alarm (3.85%) and missed detection (3.06%) rates.
- The enhancement of system interpretability through a multi-stage DL approach, distinguishing it from monolithic DL models. This distinctive feature substantially diminishes the 'black box' nature often associated with DL systems.
- The integration of DL techniques to dynamically estimate the energy detection threshold. To the best of our knowledge, although AI-based methods for spectrum sensing exist, the utilization of DL techniques to adaptively determine the threshold in energy detection has not been extensively explored in the literature; thus, it represents a novel contribution.
- Our exclusive use of the time domain samples eliminates the need for typically resource-intensive operations and transformations, although it presents additional challenges. Certain transformations excel at extracting valuable features, some of which exhibit remarkable performance even under severe channel impairments. Nonetheless, our system effectively addresses these challenges within the time domain.
- The exploration of diverse DL architectures, expanding beyond conventional choices such as CNN and LSTM. The incorporation of autoencoders serves as a bridge toward the wider integration of generative AI for the future in solving spectrum sensing problems.

The subsequent sections are organized as follows: Section 2 provides a comprehensive overview of the system model, energy detection, proposed neural network architectures, training and testing datasets, hardware setup, hyperparameter settings, as well as the block bootstrapping method, which is one of the various methods utilized for performance measurement. Section 3 presents the results obtained from the experimental analysis. Finally, Section 4 concludes the paper by discussing the findings in detail and highlighting their implications.

## 2. Materials and Methods

Although various methods in the literature extend beyond mere channel occupancy detection, spectrum sensing fundamentally aims to determine EM channel occupancy, essentially reducing to binary hypothesis testing [32]. In the following section, we present the mathematical representation of the spectrum sensing scenario.

### 2.1. Mathematical Representation of the Spectrum Sensing Scenario

The spectrum sensing scenario that we consider can be mathematically represented as:

$$\mathbf{y} = \begin{cases} \mathbf{w} & \text{if } H_0 \\ \mathbf{x} \cdot e^{j(2\pi f_\Delta n + \phi)} + \mathbf{w} & \text{if } H_1 \end{cases} \tag{1}$$

where $\mathbf{y} \in \mathbb{C}^N$ represents the vector of received samples; $\mathbf{x} \in \mathbb{C}^N$ represents the vector of transmitted signal samples; $f_\Delta$ represents the carrier frequency offset (CFO) expressed in terms of data rate; $n$ represents the zero-based array index; $\phi$ represents the phase offset in radians; $\mathbf{w} \in \mathbb{C}^N$ represents the vector of independent and identically distributed additive white Gaussian noise (AWGN) samples, where $\mathbf{w}$ follows a complex Gaussian distribution $\mathbb{CN}(\mathbf{0}, \sigma^2 \mathbf{I})$; $H_0$ denotes the null hypothesis indicating the vacancy of the channel; and, finally, $H_1$ denotes the alternative hypothesis representing channel occupancy.

### 2.2. Binary Hypothesis Testing and Energy Detection

The received signal samples, denoted as $\mathbf{y}$, are utilized to construct the test statistic $T$ according to Equation [32]:

$$T = \frac{1}{N} \sum_{n=0}^{N-1} |y[n]|^2 \tag{2}$$

Subsequently, this test statistic is compared with a threshold $\gamma$ to facilitate the hypothesis test:

$$T \underset{H_1}{\overset{H_0}{\lessgtr}} \gamma \tag{3}$$

In Equation (3), $\gamma$ represents the decision threshold, dictated by the channel's noise variance. It can be predefined or statistically estimated, and it plays a crucial role in achieving accurate and reliable detection results.

### 2.3. Proposed Adaptive Thresholding Approach

Motivated by the principle of energy conservation, we adopt a perspective that centers around Equation (1) in the following manner:

$$E_{\mathbf{y}} = \begin{cases} E_{\mathbf{w}} & \text{if } H_0 \\ E_{\mathbf{x}} + E_{\mathbf{w}} & \text{if } H_1 \end{cases} \tag{4}$$

Here, $E$ represents energy, and the subscripts denote the corresponding signal vectors. By leveraging insights from [33–35], we propose a deep learning-based method to estimate $\mathbf{x}$ from $\mathbf{y}$. This estimation allows us to determine $E_{\mathbf{x}}$, which, in turn, enables us to adaptively determine the threshold $\gamma$, which, in this case, is equivalent to $E_{\mathbf{w}}$.

Thus, Equation (3) can be reformulated by substituting $E_{\mathbf{y}}$ and $E_{\mathbf{w}}$ while introducing a correction factor $k$, as follows:

$$E_{\mathbf{y}} \underset{H_1}{\overset{H_0}{\lessgtr}} k \cdot E_{\mathbf{w}} \tag{5}$$

Introducing the correction factor $k$ addresses limitations in accurately estimating the transmitted signal vector's energy. Under the null hypothesis, where the signal vector consists of zeros, ideal estimation yields zero energy. However, inherent imperfections lead to estimates close to zero but not precisely zero. This discrepancy requires accounting for and is addressed by introducing the correction factor $k$ to adjust the threshold.

### 2.4. System Design

As shown in Equation (1), RF impairments, such as CFO, phase offset, and AWGN, affect the transmitted signal, causing deviations in the received signal. Addressing and compensating for these impairments enables accurate estimation of the transmitted signal from the received one.

We propose a multi-stage DL system that combines explicit and implicit estimation approaches to address these impairments. A dedicated neural network (NN) model

estimates the CFO, and this estimation is used with signal processing techniques to mitigate its effect on the received signal.

For the remaining impairments, such as phase offset and AWGN, an implicit estimation approach is adopted. Another dedicated neural network jointly estimates and corrects these impairments by capturing complex patterns and dependencies in the data. Training on a moderately diverse dataset, the network learns to implicitly estimate and compensate for the combined effect of phase offset and noise.

By referring to Figure 1 and following the sequential numbering assigned to each line, readers can effortlessly navigate and comprehend the system design. The system begins by estimating the CFO using a dedicated fully convolutional network (FCN). The estimated CFO is then utilized in the CFO correction block, where the received signal **y** is multiplied by $e^{-j2\pi \hat{f}_\Delta n}$ to obtain an intermediate signal $\hat{\mathbf{z}}$, which undergoes a certain level of CFO correction. This stage is known as coarse CFO estimation and correction.
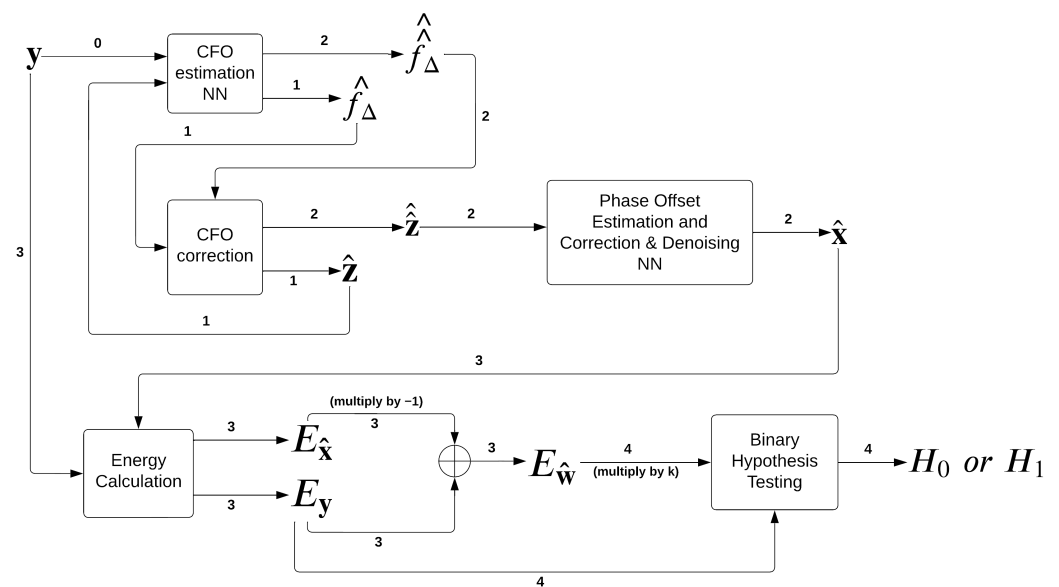


**Figure 1.** System design diagram.

Subsequently, the same FCN is employed, with the previous network's output, i.e., the CFO-corrected intermediate signal $\hat{\mathbf{z}}$, serving as the input. This stage, referred to as fine CFO estimation and correction, further refines the CFO estimation and yields the signal $\hat{\hat{\mathbf{z}}}$, which represents a well-CFO-corrected signal. The coarse estimation result is denoted as $\hat{f}_\Delta$, while the fine estimation result is denoted as $\hat{\hat{f}}_\Delta$.

Afterwards, a U-Net [36]-based autoencoder, known for its effectiveness in noise mitigation applications [37–39], is employed to compensate for phase offset and denoise the signal.

Next, the energies of both the received signal **y** and the estimated transmitted signal $\hat{\mathbf{x}}$ are computed, as depicted in Figure 1. These energy values are utilized to determine the energy of the noise $E_{\hat{\mathbf{w}}}$. Finally, the estimated noise energy is multiplied by a factor $k$, and together with $E_{\mathbf{y}}$, it is employed in the binary hypothesis testing to make a decision between $H_0$ and $H_1$.

Determining the value of parameter $k$ through an exhaustive search, covering all real values from one to infinity, and selecting the optimal $k$ where the probabilities of false alarm and missed detection intersect is theoretically valid. However, implementing such an approach is computationally infeasible. Therefore, we employ a practical and empirical method to determine an appropriate value for $k$. Specifically, we create a vector of 200 evenly spaced numbers ranging from 1 to 1.5, with the upper limit of 1.5 chosen based on empirical analysis. This approach allows for an efficient and effective selection of the parameter $k$. Each element of this vector is substituted for $k$, and the corresponding

false alarm and missed detection rates are evaluated. The values of $k$ that resulted in the intersection of the false alarm and missed detection rates are identified as the most favorable choice, as demonstrated in Figure 2. The average central processing unit time required to perform this process is approximately 800 ms.
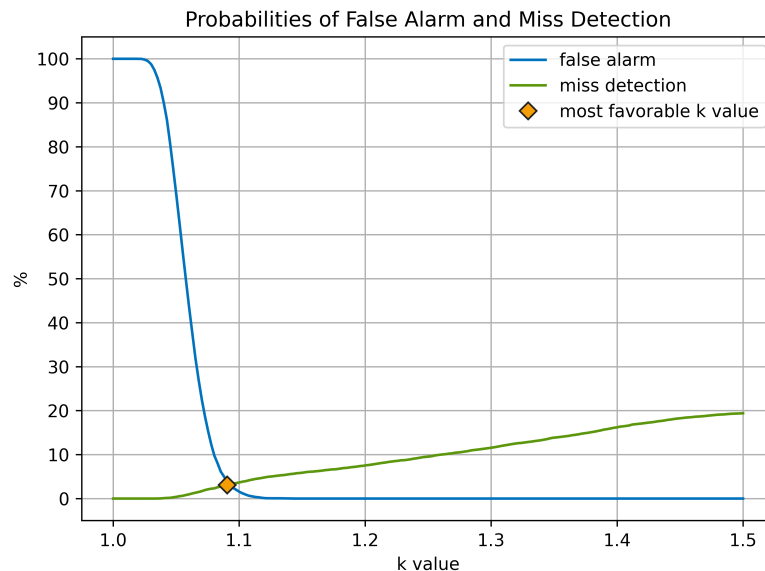


**Figure 2.** False alarm and missed detection rates as a function of k values.

While recurrent neural networks (RNNs) are commonly used for time series problems, CNNs and FCNs have also proven effective [40–43]. In our system, we employ FCNs for CFO estimation due to their ability to detect and combine complex patterns, making them suitable for this task.

Table 1 provides a comprehensive summary of the FCN layers and their associated parameters utilized for CFO estimation.

**Table 1.** Overview of fully convolutional network (FCN) layers and parameters for carrier frequency offset (CFO) estimation.

| Block | Input ($C_{in}, L$) | Output ($C_{out}, L$) | Parameters |
|---|---|---|---|
| Conv1d | (2, 512) | (32, 512) | Kernel size = 3, Stride = 1, Padding = 1 |
| MaxPool1d | (32, 512) | (32, 256) | Kernel size = 2, Stride = 2, Padding = 0 |
| Conv1d | (32, 256) | (64, 256) | Kernel size = 3, Stride = 1, Padding = 1 |
| MaxPool1d | (64, 256) | (64, 128) | Kernel size = 2, Stride = 2, Padding = 0 |
| Conv1d | (64, 128) | (128, 128) | Kernel size = 3, Stride = 1, Padding = 1 |
| MaxPool1d | (128, 128) | (128, 64) | Kernel size = 2, Stride = 2, Padding = 0 |
| Conv1d | (128, 64) | (1, 64) | Kernel size = 1, Stride = 1, Padding = 0 |
| AdaptiveAvgPool1d | (1, 64) | (1, 1) | |

The implementation is conducted using the PyTorch framework. The model has 31,265 trainable parameters.

The architecture of our U-Net-based autoencoder, which has 165,378 trainable parameters, can be seen in Figure 3.

During the training stage for both networks, a mean square error loss function was utilized.
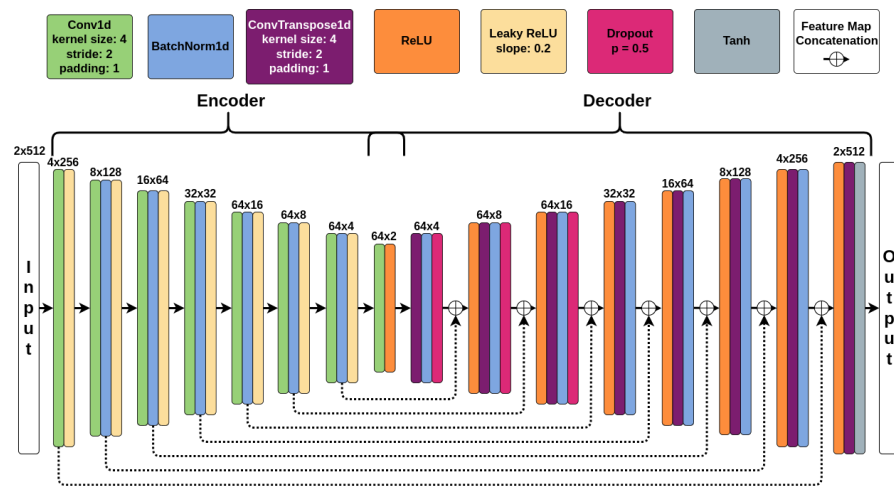
**Figure 3.** U-Net based autoencoder architecture.

## 2.5. Dataset Descriptions

In our simulations, we utilize quadrature phase-shift keying (QPSK) modulated baseband signals with a length of 512 samples. Each symbol within the signal consists of 8 samples. For pulse shaping, we utilize a square-root raised cosine filter with a roll-off factor of 0.25 and a span of 10. To simplify the analysis and implementation, we set the sampling frequency to 1 in our simulations.

During the training of the CFO network, we utilize CFO values that are uniformly distributed within the range of $[-0.01, 0.01]$ relative to the data rate. To simplify the training process, we keep the phase offset and SNR constant. The constant phase offset was chosen because it should not have an affect on the CFO estimation. Moreover, we use a relatively high SNR of 20 dB to enable the network to effectively learn the patterns caused by the CFO. Our training dataset comprises 20,000 signals, each of which consists of 512 samples with in-phase and quadrature components. We partition this dataset into 70% for training and 30% for validation. For ease of training, we normalize the CFO values to fall within the range of $[-1, 1]$, simplifying their use as target variables in the network. Additionally, we generate a separate test dataset consisting of 20,000 signals. This test dataset introduces phase offset values that are uniformly distributed from $-45$ to 45 degrees in 10-degree increments and SNR values that are uniformly distributed from 0 to 20 dB in 5 dB steps.

Table 2 provides a concise summary of the datasets utilized for both training and testing the CFO estimation network.

**Table 2.** Summary of datasets used for CFO estimation network training and testing.

| Set | CFO (Data Rate) | Phase Offset (Degrees) | SNR (dB) | Size |
|---|---|---|---|---|
| Training | $[-0.01, 0.01]$ | 30 | 20 | 20,000 |
| Test | $[-0.01, 0.01]$ | $[-45:10:45]$ | $[0:5:20]$ | 20,000 |

The training and testing datasets for the U-Net-based autoencoder are presented in Table 3, following a similar fashion as the CFO estimation dataset.

**Table 3.** Summary of datasets used for U-Net-based autoencoder network training and testing.

| Set | CFO (Data Rate) | Phase Offset (Degrees) | SNR (dB) | Size |
|---|---|---|---|---|
| Training | $[-0.01, 0.01]$ | $[-45:10:45]$ | $[0:5:20]$ | 20,000 |
| Test | $[-0.01, 0.01]$ | $[-45:10:45]$ | $[0:5:20]$ | 20,000 |

During the training of the U-Net-based autoencoder network, the trained CFO estimation network is used for CFO correction. This involves mitigating CFO in the data with

estimated values before U-Net training. It is important to note that some residual CFO remains due to estimation limitations. This approach mimics real-world scenarios with residual CFO, enhancing the U-Net's ability to handle remaining CFO components and improve practical performance.

Before discussing training and testing setups, we must describe the energy detection dataset. It consists of 10,000 signals with RF impairments, generated as previously explained. Additionally, 10,000 noise vectors following the complex normal distribution represent scenarios where the null hypothesis cannot be rejected. These sub-datasets are merged to form the final dataset for energy detection.

### 2.6. Training and Testing Setup

The training and testing of both networks were conducted on a machine equipped with an Intel i7-6700HQ CPU (8 cores) running at 2.6 GHz base frequency, an NVIDIA GeForce GTX 950M GPU, and 16 GB RAM. The CFO network underwent training for 90 epochs, employing a learning rate of $10^{-3}$. To enhance the learning process, a learning rate scheduler known as ReduceLROnPlateau was utilized, reducing the learning rate by a factor of 0.5 with a patience of 10. The Adam optimizer was employed with the same learning rate and optimizer parameters were set to $\beta_1 = 0.5$ and $\beta_2 = 0.999$.

Similarly, the U-Net-based autoencoder network was trained for 35 epochs, employing the same learning rate and Adam optimizer parameters. However, the patience value for the learning rate scheduler was adjusted to 5. This configuration facilitated effective network training and optimization of model performance.

Table 4 provides a concise summary of the training hyperparameters utilized in our study.

**Table 4.** Summary of training hyperparameters.

| Neural Network | Number of Epochs | Learning Rate | Learning Rate Scheduler | Factor | Patience | Optimizer |
|---|---|---|---|---|---|---|
| CFO Estimation | 90 | 0.001 | ReduceLR OnPlateau | 0.5 | 10 | Adam, $\beta_1 = 0.5$, $\beta_2 = 0.999$ |
| U-Net-Based Autoencoder | 35 | 0.001 | ReduceLR OnPlateau | 0.5 | 5 | Adam, $\beta_1 = 0.5$, $\beta_2 = 0.999$ |

With the hardware setup detailed in Table 5, our trained neural network can efficiently execute a single CFO estimation and correction event for an individual signal in approximately 0.6 ms. Furthermore, the other neural network can perform phase offset estimation, correction, and denoising for the same signal in approximately 2.2 ms.

**Table 5.** Summary of training and testing hardware.

| Hardware Component | Value |
|---|---|
| CPU | Intel i7-6700HQ (8 Cores) 2.6 GHz |
| GPU | GeForce GTX 950M |
| RAM | 16 GB |

### 2.7. Block Bootstrapping

To evaluate the performance of our system, we utilized various assessment methods. One of these methods involves employing the block bootstrapping technique [44] to construct 95% prediction intervals, which are presented in Section 3 afterwards. This method is applied individually to each signal estimation. Initially, we computed the corresponding residuals by computing the differences between our estimate and the true transmitted signal. Then, we generated multiple blocks of length 81 by striding over the residuals vector with a stride of 1, extracting a block at each stride. These blocks were then randomly

sampled with replacement, concatenated, and trimmed to the length of 512. This process was repeated multiple times, resulting in the construction of 3000 residual vectors in our simulation.

To obtain the 95% prediction interval for the corresponding estimation, we added each of the residual vectors to our estimation one at a time. This process resulted in the formation of a new dataset. Finally, we computed the 2.5th and 97.5th percentiles of this dataset, which served as the lower and upper bounds of the prediction interval, respectively.

The utilization of the block bootstrapping method is preferred over naive resampling approaches due to the interdependence of contiguous samples in our transmitted signal, and consequently the estimated signal, caused by the pulse shaping filter. By attempting to mimic the underlying process that generated the time series, such as the residuals in our case, the block bootstrapping method aims to capture the temporal dependencies.

The choice of block length is a critical factor in block bootstrapping, as it directly impacts the ability of the method to capture the desired temporal dependencies. It serves as a tunable parameter, and an inappropriate selection of the block length may hinder the effectiveness of block bootstrapping in capturing the intended dependencies. In our case, we chose a block length of 81 to align with the length of our pulse shaping filter, ensuring that relevant dependencies within the signal were properly captured.

## 3. Results

The presence of RF impairments in the received signal and their subsequent mitigation to obtain an estimate of the transmitted signal had a profound impact on the performance of our energy detection system, particularly in the determination of the threshold. Therefore, our initial evaluation focuses on assessing the performance of the two neural networks responsible for mitigating these RF impairments. Following the evaluation of the neural networks involved in RF impairment mitigation, we proceed to present the evaluation metrics for energy detection.

### 3.1. CFO Estimation

Figure 4 illustrates the Mean Absolute Error (MAE) between the normalized true CFO and the estimated CFO, considering different SNR and phase offset values. The results demonstrate a noticeable improvement in performance as the fine estimation follows the coarse estimation, leading to a reduction in the MAE. Consistent with our expectations, higher SNR values correspond to lower MAE values, indicating improved CFO estimation. Furthermore, the results confirm that phase offset has a negligible impact on CFO estimation, aligning with our prior understanding.
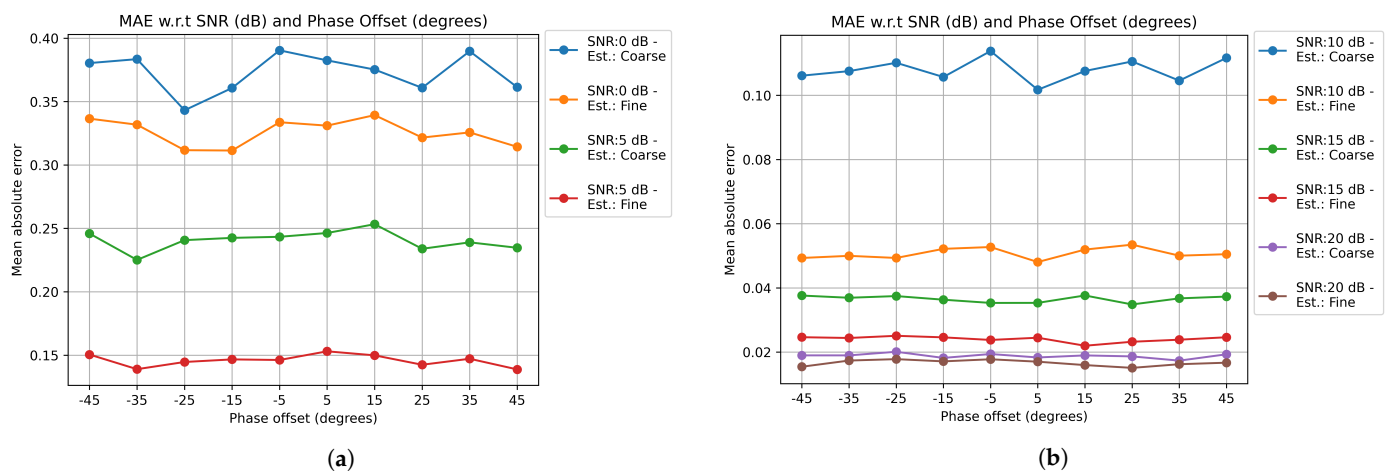


**Figure 4.** CFO estimation results. (**a**) Mean Absolute Error (MAE) between the true CFO and estimated CFO for $[0, 5]$ dB Signal-to-Noise Ratio (SNR). (**b**) MAE between the true CFO and estimated CFO for $[10, 20]$ dB SNR.

### 3.2. Transmitted Signal Estimation

Figure 5 presents the results for randomly selected signals at various SNR levels, including the true transmitted signal (blue), the estimated transmitted signal (red), and the corresponding 95% prediction interval (gray). In the previous subsection focusing on CFO estimation, we established an inverse relationship between the SNR and MAE, indicating that higher SNR values lead to lower CFO estimation errors. Expanding on this observation, Figure 5 reveals that the combined effect of low SNR and the inferior quality of CFO estimation at lower SNR levels, in comparison with higher SNR levels, leads to a decrease in the performance of the transmitted signal estimation. On the other hand, the inverse is also true, where higher SNR levels and improved CFO estimation contribute to enhanced performance in signal estimation.

(a)

(b)

(c)
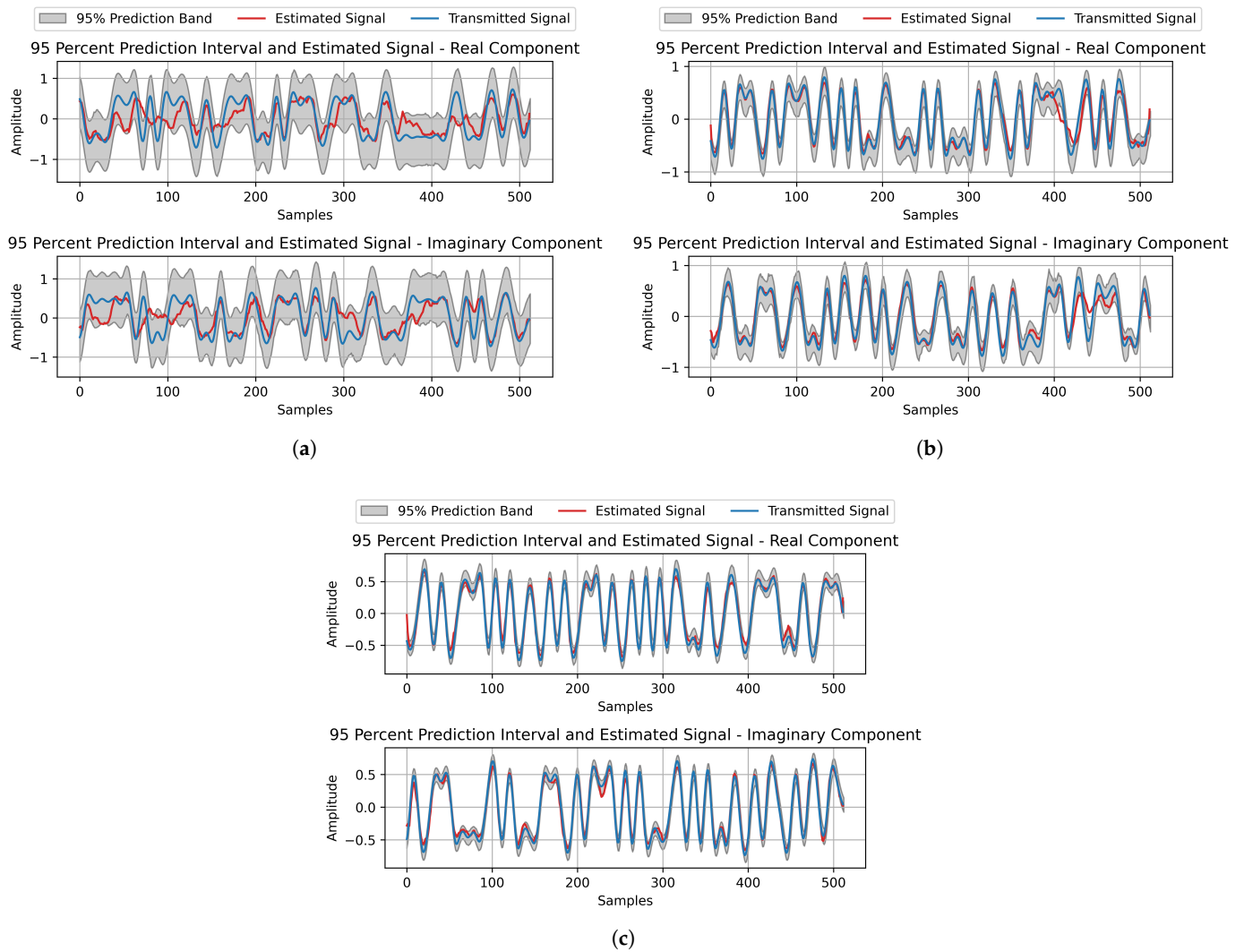
**Figure 5.** Transmitted signal estimation results. (**a**) A randomly selected estimation result of the transmitted signal at 0 dB. (**b**) A randomly selected estimation result of the transmitted signal at 10 dB. (**c**) A randomly selected estimation result of the transmitted signal at 20 dB.
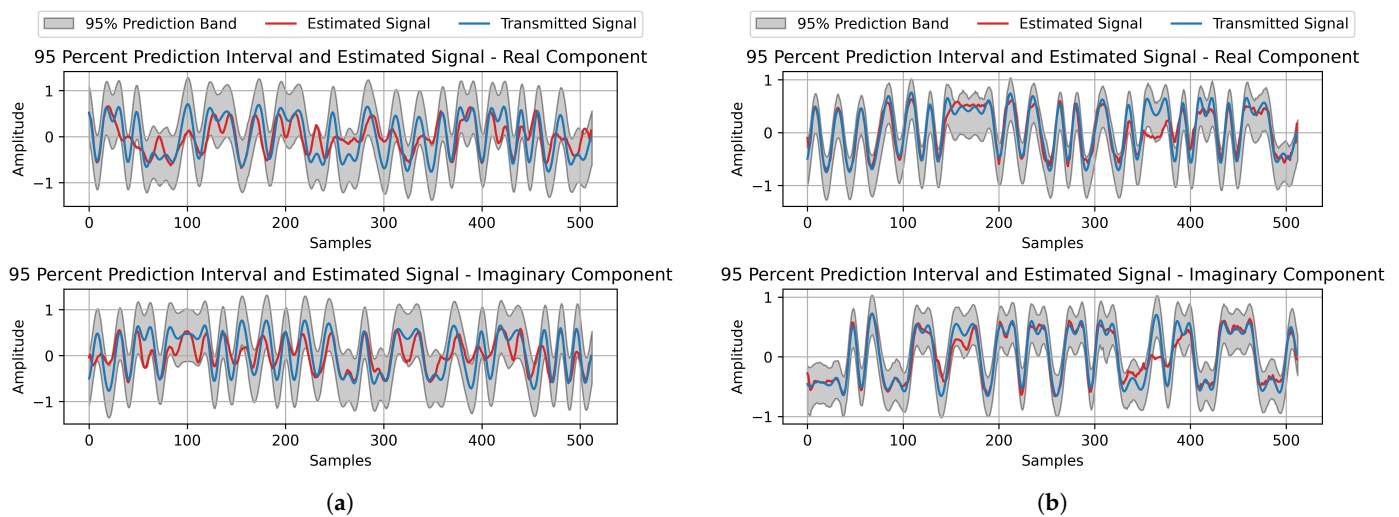
Table 6 provides an overview of the RF impairments present in each of the signals presented in Figure 5.

**Table 6.** Radio Frequency (RF) impairments that are present in each of the signals provided in Figure 5.

| Subfigure | True CFO | CFO Est. | \| True CFO − Est. CFO \| | SNR (dB) | Phase Offset (degrees) |
|---|---|---|---|---|---|
| (a) | 0.5143 | 0.3229 | 0.1914 | 0 | 15 |
| (b) | 0.5429 | 0.4987 | 0.0442 | 10 | -25 |
| (c) | 0.4768 | 0.4827 | 0.0059 | 20 | 35 |

CFO values are rounded to 4 decimal places.

While the estimation performance of the transmitted signal is indeed satisfactory at high SNR levels, it is important to note that it is not solely determined by the SNR. Figure 6a provides a clear example of this, where, despite an SNR of 20 dB, the transmitted signal estimation performance is poor. This can be attributed to a phase offset of 45 degrees, as the QPSK symbol constellations become indistinguishable from the baseband signal observations at ±45 degrees. Furthermore, it is essential to acknowledge the presence of outliers in the estimation results. Figure 6b highlights cases where the transmitted signal estimation performance is poor, particularly when there is no phase offset of ±45 degrees. These outliers, although relatively infrequent, do not significantly impact the overall system performance. We demonstrate this by presenting the results that follow.



**Figure 6.** Transmitted signal estimation results—outliers. (**a**) Example of the estimated transmitted signal at 20 dB with a phase offset of 45 degrees. (**b**) Outlier example of the estimated transmitted signal at 20 dB with a phase offset that is not ±45 degrees.

Table 7 provides a breakdown of the RF impairments present in each of the signals featured in Figure 6.

**Table 7.** RF impairments that are present in each of the signals provided in Figure 6.

| Subfigure | True CFO | CFO Est. | \| True CFO − Est. CFO \| | SNR (dB) | Phase Offset (degrees) |
|---|---|---|---|---|---|
| (a) | 0.9196 | 0.9200 | 0.0004 | 20 | 45 |
| (b) | 0.1057 | 0.1639 | 0.0582 | 20 | −15 |

CFO values are rounded to 4 decimal places.

The assessment of the overall performance of the U-Net-based autoencoder neural network cannot be effectively conducted by visually inspecting individual pairs of true and estimated transmitted signals. To address this, we adopt a quantitative approach by computing the residuals between the true transmitted signal and the received signal, as

well as between the true transmitted signal and the estimated transmitted signal, for each signal in our dataset. Subsequently, we calculate the average energy of the residuals for both cases. Figure 7a illustrates the relationship between the SNR and the energy of the residuals. As anticipated, an increase in the SNR corresponds to a decrease in the energy of the residuals. Furthermore, the figure demonstrates that the average energy of the residuals between the true transmitted and estimated transmitted signal is significantly lower than the average energy of the residuals between the true transmitted and received signal. This observation strongly suggests that the good performance of the estimation leads to reduced residuals.



(a)



(b)



(c)
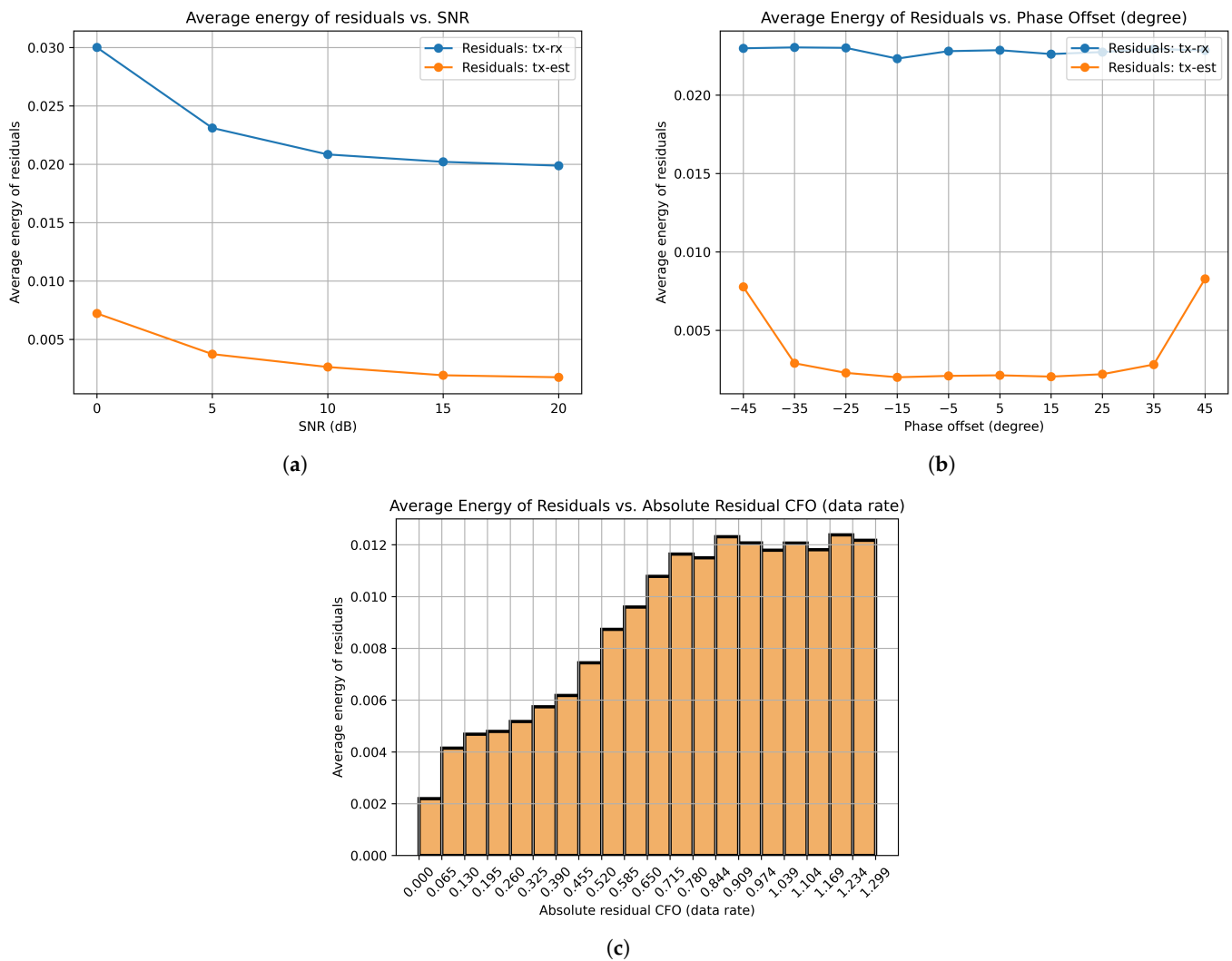
**Figure 7.** Average energy of residuals with respect to RF impairments. (**a**) Average energy of residuals with respect to SNR. (**b**) Average energy of residuals with respect to phase offset. (**c**) Average energy of residuals with respect to absolute residual CFO.

Figure 7b presents the average energy of the residuals in relation to the phase offset. Consistent with previous discussions, we observe that the estimation performance is notably poor when the phase offset is ±45 degrees. Furthermore, upon examination of this figure, it becomes evident that the scenario depicted in Figure 6b represents an outlier case. As previously discussed, the presence of outliers does not significantly impact the overall performance of our system. Lastly, Figure 7c illustrates the relationship between the average energy of residuals, specifically those between the true transmitted signal and the estimated transmitted signal, and the absolute residual CFO. The absolute residual CFO is computed as the absolute difference between the true CFO and the estimated CFO. As

anticipated, a clear direct relationship is observed: as the absolute residual CFO increases, the average energy of the residuals also increases.

### 3.3. Energy Detection

In this section, we exhibit the performance of the energy detector using the optimal k value. Figure 8 provides an extensive performance analysis using a dataset of 20,000 signals. Among these, 10,000 signals signify channel occupancy, while the remaining 10,000 represent spectrum availability. The subset denoting channel occupancy spans a range of SNR levels from 0 dB to 20 dB, with intervals of 5 dB. Following the application of our proposed system for channel impairment mitigation, the results reveal a false alarm rate of 3.85% and a missed detection rate of 3.06%. These quantitative findings distinctly validate the effectiveness of our approach.

Figure 9, on the other hand, provides insights into the system's performance across varying $k$ values. While typical receiver operating characteristic (ROC) curves depict model performance at different classification thresholds, our approach dynamically adjusts the threshold based on the $k$ value. Given the significance of finding the optimal $k$ value for peak performance, our ROC curve illustrates how different $k$ values influence the results.
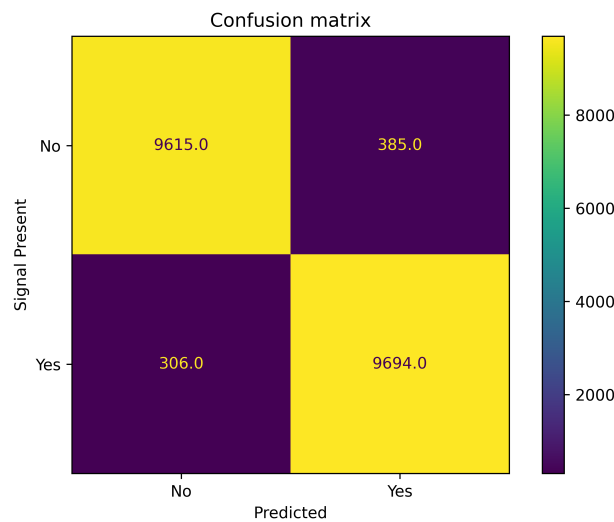


**Figure 8.** Confusion matrix analysis of the energy detector performance using the best k value.
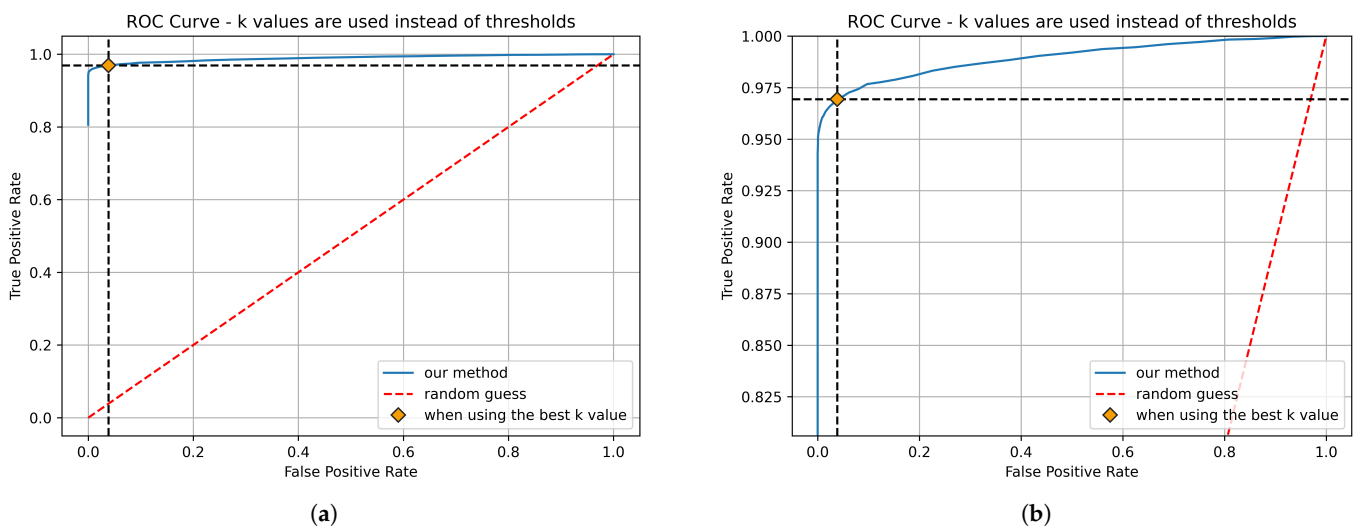


**Figure 9.** Receiver operating characteristic (ROC) curves. (**a**) Original ROC curve. (**b**) Zoomed-in ROC curve for better visualization.

## 4. Discussion and Conclusions

Spectrum sensing encompasses numerous aspects, with one fundamental yet critical challenge being the balance between computational complexity and performance. This study proposes a multistage approach that employs DL to adaptively estimate the energy detector threshold by utilizing only the time domain representation of received signal samples. The aim is to achieve a delicate equilibrium between computational complexity and performance.

The proposed model distinguishes itself through its simplicity, relying exclusively on time domain samples affected by RF impairments, thus avoiding the need for additional feature extraction operations or transformations. It is noteworthy that some transformations excel at extracting valuable features, even in the presence of severe channel impairments. Therefore, abstaining from their use presents additional challenges. Nevertheless, our system effectively tackles these challenges within the time domain, achieving outstanding performance with low false alarm (3.85%) and missed detection (3.06%) rates, all while jointly mitigating channel impairments and conducting spectrum sensing.

We leverage the received samples, which are influenced by RF impairments, to estimate the transmitted signal. By estimating the energies of both the transmitted and received signals, we can compute the noise energy necessary for threshold estimation. This noise energy is then multiplied by a correction factor, denoted as k, to further refine the threshold estimation process.

The multistage approach incorporates an FCN for accurate CFO estimation and explicit CFO correction. Phase offset estimation, correction, and noise suppression are implicitly handled by a U-Net-based autoencoder network. Energy calculations are performed on the received and estimated transmitted signals to estimate the noise energy. Finally, the energy of the received signal and the k-adjusted noise energy are used for binary hypothesis testing, enabling effective spectrum sensing. Quantitative analyses confirm the efficacy of our proposed method.

Based on our literature research, although AI-based methods for spectrum sensing are available, the application of DL techniques for dynamically determining the energy detection threshold has not been comprehensively investigated in the existing literature. This represents a unique and innovative contribution of our work.

We also investigate a range of DL architectures, going beyond the typical selections, such as CNN and LSTM. The inclusion of autoencoders serves as a gateway to the broader integration of generative AI, a path to potentially improving spectrum sensing in the future.

We acknowledge the limitations of our approach. The system's performance degrades when encountering phase offsets exceeding 45 degrees, making it less suitable for complex modulation schemes like 16-QAM or 64-QAM, as well as presenting additional challenges in accurate detection and parameter estimation when applied to signals conforming to standards like LTE and 5G NR, which exhibit noise-like properties.

Motivated by the identified limitations, we propose several potential research directions to address the challenges. One immediate but challenging approach is to design custom loss functions specifically tailored to train the neural networks. The customized loss functions would incorporate various characteristics of the received signal, particularly its statistical properties. By incorporating relevant statistical information into the training process, we anticipate that the neural networks could better adapt to the inherent complexities and variations present in the received signal, ultimately improving the overall system performance. However, developing such custom loss functions would require careful consideration and exploration of appropriate statistical metrics and techniques, making it a challenging yet promising avenue for further investigation. In addition to exploring custom loss functions, another promising research direction is to investigate the integration of state-of-the-art DL techniques into the proposed system. Techniques such as attention mechanisms [45] and diffusion models [46] have shown significant advancements in various domains and have the potential to enhance the mitigation of RF impairments. A more robust approach would involve leveraging cyclostationary or covariance-based

features, which provide valuable information about the underlying signal structure. However, extracting these features traditionally requires significant computational resources. Therefore, a promising research direction is to explore DL methods for estimating these features directly from the received samples. This approach would involve developing specialized architectures and training techniques to efficiently extract informative features and enhance system performance.

In our future work, we intend to conduct real-world experiments to validate the system's performance under practical conditions. Furthermore, we aim to explore various use case scenarios and implement necessary modifications to extend the system's applicability to more complex modulation schemes and signals that adhere to specific wireless communication standards.

**Author Contributions:** Conceptualization, O.B., A.R.E. and M.K.O.; methodology, O.B.; software, O.B.; validation, O.B., A.R.E. and M.K.O.; formal analysis, O.B.; investigation, O.B.; resources, O.B., A.R.E. and M.K.O.; data curation, O.B.; writing—original draft preparation, O.B.; writing—review and editing, A.R.E. and M.K.O.; visualization, O.B.; supervision, A.R.E. and M.K.O.; project administration, A.R.E. and M.K.O.; funding acquisition, A.R.E. and M.K.O. All authors have read and agreed to the published version of the manuscript.

**Data Availability Statement:** The data presented in this study are available on request from the corresponding author.

**Conflicts of Interest:** The authors declare no conflict of interest.

## Abbreviations

The following abbreviations are used in this manuscript:

| | |
|---|---|
| DL | Deep Learning; |
| RF | Radio Frequency; |
| CFO | Carrier Frequency Offset; |
| AWGN | Additive White Gaussian Noise; |
| EM | Electromagnetic; |
| MIMO | Multiple-Input Multiple-Output; |
| CR | Cognitive Radio; |
| SNR | Signal-to-Noise Ratio; |
| AI | Artificial Intelligence; |
| NN | Neural Network; |
| FCN | Fully Convolutional Network; |
| RNN | Recurrent Neural Network; |
| CNN | Convolutional Neural Network; |
| QPSK | Quadrature Phase-Shift Keying; |
| MAE | Mean Absolute Error; |
| ROC | Receiver Operating Characteristic; |
| LSTM | Long Short-Term Memory; |
| BiLSTM | Bidirectional Long Short-Term Memory; |
| SA | Self-Attention; |
| SMT | Spectral Minima Tracking. |

## References

1. Agiwal, M.; Roy, A.; Saxena, N. Next Generation 5G Wireless Networks: A Comprehensive Survey. *IEEE Commun. Surv. Tuts.* **2016**, *18*, 1617–1655. [CrossRef]
2. Haykin, S. Cognitive Radio: Brain-Empowered Wireless Communications. *IEEE J. Sel. Top. Signal Process.* **2005**, *23*, 201–220. [CrossRef]
3. Hassanien, A.; Amin, M.G.; Aboutanios, E.; Himed, B. Dual-function radar communication systems: A solution to the spectrum congestion problem. *IEEE Signal Process. Mag.* **2019**, *36*, 115–126. [CrossRef]

4.	Liu, F.; Cui, Y.; Masouros, C.; Xu, J.; Han, T.X.; Eldar, Y.C.; Buzzi, S. Integrated Sensing and Communications: Toward Dual-Functional Wireless Networks for 6G and Beyond. *IEEE J. Sel. Areas Commun.* **2022**, *40*, 1728–1767. [CrossRef]

5.	Zhang, J.A.; Liu, F.; Masouros, C.; Heath, R.W.; Feng, Z.; Zheng, L.; Petropulu, A. An Overview of Signal Processing Techniques for Joint Communication and Radar Sensing. *IEEE J. Sel. Top. Signal Process.* **2021**, *15*, 1295–1315. [CrossRef]

6.	Sharma, S.K.; Chatzinotas, S.; Ottersten, B. Transmit Beamforming for Spectral Coexistence of Satellite and Terrestrial Networks. In Proceedings of the 8th International Conference on Cognitive Radio Oriented Wireless Networks, Washington, DC, USA, 8–10 July 2013; pp. 275–281. [CrossRef]

7.	Lu, L.; Li, G.Y.; Swindlehurst, A.L.; Ashikhmin, A.; Zhang, R. An Overview of Massive MIMO: Benefits and Challenges. *IEEE J. Sel. Top. Signal Process.* **2014**, *8*, 742–758. [CrossRef]

8.	Mitola, J.; Maguire, G.Q. Cognitive Radio: Making Software Radios More Personal. *IEEE Pers. Commun.* **1999**, *6*, 13–18. [CrossRef]

9.	Akyildiz, I.F.; Lee, W.; Vuran, M.C.; Mohanty, S. Next Generation/Dynamic Spectrum Access/Cognitive Radio Wireless Networks: A Survey. *Comput. Netw.* **2006**, *50*, 2127–2159. [CrossRef]

10.	Liang, Y.C.; Chen, K.C.; Li, G.Y.; Mahonen, P. Cognitive Radio Networking and Communications: An Overview. *IEEE Trans. Veh. Technol.* **2011**, *60*, 3386–3407. [CrossRef]

11.	Yucek, T.; Arslan, H. A Survey of Spectrum Sensing Algorithms for Cognitive Radio Applications. *IEEE Commun. Surv. Tutor.* **2009**, *11*, 116–130. [CrossRef]

12.	Koziol, M. 5G Networks Are Performing Worse. What Is Going on? Available online: https://spectrum.ieee.org/5g-rollout-disappointments (accessed on 22 May 2023).

13.	Zhang, Z.; Xiao, Y.; Ma, Z.; Xiao, M.; Ding, Z.; Lei, X.; Karagiannidis, G.K.; Fan, P. 6G Wireless Networks: Vision, Requirements, Architecture, and Key Technologies. *IEEE Veh. Technol. Mag.* **2019**, *14*, 28–41. [CrossRef]

14.	Saad, W.; Bennis, M.; Chen, M. A Vision of 6G Wireless Systems: Applications, Trends, Technologies, and Open Research Problems. *IEEE Netw.* **2020**, *34*, 134–142. [CrossRef]

15.	Ali, A.; Hamouda, W. Advances on spectrum sensing for cognitive radio networks: Theory and applications. *IEEE Commun. Surv. Tutor.* **2017**, *19*, 1277–1304. [CrossRef]

16.	Arjoune, Y.; Kaabouch, N. A comprehensive survey on Spectrum Sensing in cognitive radio networks: Recent advances, new challenges, and future research directions. *Sensors* **2019**, *19*, 126. [CrossRef] [PubMed]

17.	Ahmad, B.I. A Survey of Wideband Spectrum Sensing Algorithms for Cognitive Radio Networks and Sub-Nyquist Approaches. *arXiv* **2020**, arXiv:2001.02574.

18.	He, A.; Bae, K.K.; Newman, T.R.; Gaeddert, J.; Kim, K.; Menon, R.; Morales-Tirado, L.; Neel, J.; Zhao, Y.; Reed, J.H.; et al. A Survey of Artificial Intelligence for Cognitive Radios. *IEEE Trans. Veh. Technol.* **2010**, *59*, 1578–1592. [CrossRef]

19.	Xie, J.; Fang, J.; Liu, C.; Li, X. Deep Learning-Based Spectrum Sensing in Cognitive Radio: A CNN-LSTM Approach. *IEEE Commun. Lett.* **2020**, *24*, 2196–2200. [CrossRef]

20.	Chen, Z.; Xu, Y.Q.; Wang, H.; Guo, D. Deep STFT-CNN for Spectrum Sensing in Cognitive Radio. *IEEE Commun. Lett.* **2021**, *25*, 864–868. [CrossRef]

21.	Tekbiyik, K.; Akbunar, O.; Ekti, A.R.; Gorcin, A.; Kurt, G.K.; Qaraqe, K.A. Spectrum Sensing and Signal Identification With Deep Learning Based on Spectral Correlation Function. *IEEE Trans. Veh. Technol.* **2021**, *70*, 10514–10527. [CrossRef]

22.	Zheng, S.; Chen, S.; Qi, P.; Zhou, H.; Yang, X. Spectrum sensing based on deep learning classification for cognitive radios. *China Commun.* **2020**, *17*, 138–148. [CrossRef]

23.	Peng, Q.; Gilman, A.; Vasconcelos, N.; Cosman, P.C.; Milstein, L.B. Robust Deep Sensing Through Transfer Learning in Cognitive Radio. *IEEE Wirel. Commun. Lett.* **2020**, *9*, 38–41. [CrossRef]

24.	Xing, H.; Qin, H.; Luo, S.; Dai, P.; Xu, L.; Cheng, X. Spectrum sensing in cognitive radio: A deep learning based model. *Trans. Emerg. Telecommun. Technol.* **2022**, *33*, e4388. [CrossRef]

25.	Gorcin, A.; Qaraqe, K.A.; Celebi, H.; Arslan, H. An Adaptive Threshold Method for Spectrum Sensing in Multi-Channel Cognitive Radio Networks. In Proceedings of the 2010 17th International Conference on Telecommunications, Doha, Qatar, 4–7 April 2010; pp. 425–429. [CrossRef]

26.	Ling, X.; Wu, B.; Wen, H.; Ho, P.H.; Bao, Z.; Pan, L. Adaptive Threshold Control for Energy Detection Based Spectrum Sensing in Cognitive Radios. *IEEE Wirel. Commun. Lett.* **2012**, *1*, 448–451. [CrossRef]

27.	Wang, N.; Gao, Y.; Zhang, X. Adaptive Spectrum Sensing Algorithm Under Different Primary User Utilizations. *IEEE Commun. Lett.* **2013**, *17*, 1838–1841. [CrossRef]

28.	Martian, A.; Al Sammarraie, M.J.A.; Vlădeanu, C.; Popescu, D.C. Three-Event Energy Detection with Adaptive Threshold for Spectrum Sensing in Cognitive Radio Systems. *Sensors* **2020**, *20*, 3614. [CrossRef]

29.	Tingting, S.; Youyun, X. Dynamic threshold spectrum sensing method based on DQN combined with clustered cooperative sensing architecture. In Proceedings of the 2023 IEEE 97th Vehicular Technology Conference (VTC2023-Spring), Florence, Italy, 20–23 June 2023; pp. 1–6. [CrossRef]

30.	Uriarte, I.; Martínez, D.M.; Andrade, Á.G.; Galaviz, G.; Barboza, N.A. Spectral minima tracking for improving the energy detection under noise power uncertainty. *Alex. Eng. J.* **2023**, *66*, 619–632. [CrossRef]

31.	Vladeanu, C.; Al-Dulaimi, O.M.K.; Martian, A. A Modified Double-Threshold Spectrum Sensing Algorithm Based on Adaptive-Threshold Mean Energy Detection. In Proceedings of the 2021 International Symposium on Signals, Circuits and Systems (ISSCS), Iasi, Romania, 15–16 July 2021; pp. 1–4. [CrossRef]

32.  Guimarães, D. Spectrum Sensing: A Tutorial. *J. Commun. Inf. Syst.* **2022**, *37*, 10–29. [CrossRef]
33.  Isola, P.; Zhu, J.Y.; Zhou, T.; Efros, A.A. Image-to-Image Translation with Conditional Adversarial Networks. In Proceedings of the 2017 IEEE Conference on Computer Vision and Pattern Recognition (CVPR), Honolulu, HI, USA, 21–26 July 2017; pp. 5967–5976. [CrossRef]
34.  Hanna, S.; Dick, C.; Cabric, D. Signal Processing Based Deep Learning for Blind Symbol Decoding and Modulation Classification. *arXiv* **2021**, arXiv:2106.10543.
35.  Shevitski, B.; Watkins, Y.; Man, N.; Girard, M. Digital Signal Processing Using Deep Neural Networks. *arXiv* **2021**, arXiv:2109.10404.
36.  Ronneberger, O.; Fischer, P.; Brox, T. U-Net: Convolutional Networks for Biomedical Image Segmentation. In Proceedings of the Medical Image Computing and Computer-Assisted Intervention—MICCAI 2015, Munich, Germany, 5–9 October 2015; Navab, N., Hornegger, J., Wells, W.M., Frangi, A.F., Eds.; Springer International Publishing: Cham, Switzerland, 2015; pp. 234–241. [CrossRef]
37.  Komatsu, R.; Gonsalves, T. Comparing U-Net Based Models for Denoising Color Images. *AI* **2020**, *1*, 465–486. [CrossRef]
38.  Jia, F.; Wong, W.H.; Zeng, T. DDUNet: Dense Dense U-Net with Applications in Image Denoising. In Proceedings of the 2021 IEEE/CVF International Conference on Computer Vision Workshops (ICCVW), Montreal, BC, Canada, 11–17 October 2021; pp. 354–364. [CrossRef]
39.  Gurrola-Ramos, J.; Dalmau, O.; Alarcón, T.E. A Residual Dense U-Net Neural Network for Image Denoising. *IEEE Access* **2021**, *9*, 31742–31754. [CrossRef]
40.  Lim, B.; Zohren, S. Time-series forecasting with Deep Learning: A Survey. *Philos. Trans. R. Soc. A Math. Phys. Eng. Sci.* **2021**, *379*, 20200209. [CrossRef]
41.  Sengupta, S.; Basak, S.; Saikia, P.; Paul, S.; Tsalavoutis, V.; Atiah, F.; Ravi, V.; Peters, A. A review of deep learning with special emphasis on architectures, applications and recent trends. *Knowl.-Based Syst.* **2020**, *194*, 105596. [CrossRef]
42.  Sezer, O.B.; Gudelek, M.U.; Ozbayoglu, A.M. Financial time series forecasting with deep learning: A systematic literature review: 2005–2019. *Appl. Soft Comput.* **2020**, *90*, 106181. [CrossRef]
43.  Torres, J.F.; Hadjout, D.; Sebaa, A.; Martínez-Álvarez, F.; Troncoso, A. Deep Learning for Time Series Forecasting: A Survey. *Big Data* **2021**, *9*, 3–21. [CrossRef]
44.  Bühlmann, P. Bootstraps for Time Series. *Stat. Sci.* **2002**, *17*, 52–72. [CrossRef]
45.  Vaswani, A.; Shazeer, N.; Parmar, N.; Uszkoreit, J.; Jones, L.; Gomez, A.N.; Kaiser, L.u.; Polosukhin, I. Attention is All you Need. In *Proceedings of the Advances in Neural Information Processing Systems*; Guyon, I., Luxburg, U.V., Bengio, S., Wallach, H., Fergus, R., Vishwanathan, S., Garnett, R., Eds.; Curran Associates, Inc.: Red Hook, NY, USA, 2017; Volume 30.
46.  Ho, J.; Jain, A.; Abbeel, P. Denoising Diffusion Probabilistic Models. In *Proceedings of the Advances in Neural Information Processing Systems*; Larochelle, H., Ranzato, M., Hadsell, R., Balcan, M., Lin, H., Eds.; Curran Associates, Inc.: Red Hook, NY, USA, 2020; Volume 33, pp. 6840–6851.